Proceedings of the
Annual Stability Conference
Structural Stability Research Council
San Antonio, Texas, March 21-24, 2017

Buckling and Collapse Behavior of Screw-Fastened, Built-Up Cold-Formed Steel Columns of Varying Cross-Section Size: Experimental Investigation

David C. Fratamico[1], Shahabeddin Torabian[2], Kim J. R. Rasmussen[3], and Benjamin W. Schafer[4]

Abstract

An ongoing experimental effort using built-up cold-formed steel (CFS) columns is discussed in this paper. The quantification of partially-composite action, determination of member end fixity, and observation of buckling and post-buckling behavior is presented. Specifically, the section studied herein is a common back-to-back, lipped channel section with two self-drilling screw fasteners connecting the webs of the individual channel sections along their length. The specimens are 6 ft (1.83 m) in height and are bound by 1 ft (305 mm) of track. Previous experimental work by the authors has focused on studying the effect of sheathing, end conditions, and fastener spacing on composite action, and a separate series of tests examined the effect of fastener layout on local and distortional buckling. The tests presented herein conclude with a study of 16 different cross-sections, where each section is tested with two web fastener layout types as determined via AISI S100 (2016) section I1.2. A total of 32 monotonic, concentric compression tests are completed with 15 position transducers monitoring displacements at key locations. Material properties and initial imperfections are quantified for each specimen before testing. Results show a vast range of deformation behavior, with local-global interaction and flexural-torsional modes common in many of the sections. End fastener groups boost capacity only when minor-axis flexural buckling is observed. Also, the column end conditions are determined to be semi-rigid, but almost fixed-fixed for all sections. Future work includes nonlinear FEA modeling validated by test data and a new design approach using finite strip-based modeling and the Direct Strength Method.

1. Introduction

1.1 Background and Current Design

Cold-formed steel (CFS) structures are mostly composed of thin-walled sections which are assembled in panels that have high axial and lateral capacities while also being lightweight. When higher local rigidity, or axial or flexural capacity are required, built-up CFS sections are often assembled and used. Built-up sections are also commonly used as chord studs in CFS-framed shear or exterior walls, headers/jambs, or truss members. Some common, simple built-up sections are the back-to-back lipped channel section and the toe-to-toe, closed "box" section. Individual CFS

[1] Ph.D. Student, Dept. of Civil Engineering, Johns Hopkins University, <fratamico@jhu.edu>
[2] Assistant Research Professor, Dept. of Civil Engineering, Johns Hopkins University <torabian@jhu.edu>
[3] Professor, School of Civil Engineering, University of Sydney, <kim.rasmussen@sydney.edu.au>
[4] Professor, Dept. of Civil Engineering, Johns Hopkins University, <schafer@jhu.edu>

studs are fastened together, and composite action can be developed via the use of screws, bolts, welds, or battens. Ongoing research conducted by the authors aims to understand this composite action and the achievable capacities over a range of built-up column cross-section types and fastening/bracing arrangements, as well as to augment current design specifications.

The 2005 AS/NZS 4600 Standard for CFS members limits only the maximum fastener spacing along the column length by ensuring that flexural buckling of the individual studs between fasteners will not occur prior to global flexural buckling of the built-up section. In the U.S., AISI S100 (2016) Section I1.2 requires the calculation of axial capacity using the modified slenderness ratio approach, which was adopted from AISC 360 (2010) and assumes only minor-axis flexural buckling in the estimation of strength, F_e. Eqs. 1 and 2 show the basis for these calculations.

$$F_e = \frac{\pi^2 E}{\left(\frac{KL}{r}\right)_m^2} \tag{1}$$

$$\left(\frac{KL}{r}\right)_m = \sqrt{\left(\frac{KL}{r}\right)_o^2 + \left(\frac{a}{r_i}\right)^2} \tag{2}$$

In Eq. 2, $(KL/r)_o$ is the slenderness ratio of the entire built-up section about its minor axis, a is the intermediate fastener spacing along the column's height, and r_i is the minimum radius of gyration of each single stud in the built-up section. This modified slenderness method estimates a loss of shear rigidity at the discrete fasteners and increases the slenderness ratio of the built-up section to reduce its capacity accordingly. The method cannot predict the effects of fastener spacing/layouts on torsional, flexural-torsional, local, or distortional buckling modes. For a complete design, local and distortional strengths are also required to be determined using the Effective Width Method (EWM) or the Direct Strength Method (DSM) on either the individual sections or the fully-composite built-up cross-section. The governing strength is the minimum stress: F_e (nominal global strength), F_l (nominal local strength), or F_d (nominal distortional strength).

$$\frac{a}{r_i} \leq \frac{1}{2}\left(\frac{KL}{r}\right) \tag{3}$$

Like the requirements in the AS/NZ code, a limitation on the fastener spacing along the length is used to ensure that individual stud buckling does not occur before the entire built-up section buckles. Eq. 3 is used to determine this maximum spacing a along the length. If the modified slenderness ratio is used in Eq. 3, an iterative calculation must be performed to obtain an optimal spacing. Although the Specification does not clarify whether the fasteners should be single or doubled within each fastener longitudinal spacing increment, the doubled configuration is conservatively assumed in the work presented in this paper. AISI S100 (2016) also requires a prescriptive fastener grouping at the member ends, but its impact on the modified slenderness is not treated directly. As per section I1.2, if screws are used as fasteners in these end fastener groups (EFG), they must be longitudinally spaced no more than 4 diameters apart and for a distance equal to 1.5 times the maximum width of the built-up section.

1.2 Related Work

Within the past decade, work has conducted to better understand the prevailing buckling modes and strength of built-up CFS columns. For example, results of column experiments using back-to-back CFS channel sections showed that the AISI S100 (2012) modified slenderness ratio can be conservative for certain plate thicknesses and that the end connections are critical for maintaining overall column strength (Stone and LaBoube 2005). Related to the work reported here, Fratamico et al. (2016) studied composite action in back-to-back built-up CFS columns using two cross-section types, sheathing, and varying web fastener layouts; results indicate a modest increase in composite action and capacity with extra web fasteners where shear slip is greatest in columns undergoing flexural buckling, and local buckling controlling in sheathed column cases.

Further, a series of tests and follow-up numerical analyses were completed at KU Leuven in which various types of built-up CFS column cross-sections using Z-shape, sigma, and track sections have been completed with mostly fixed end conditions; compression capacities were compared with DSM-based equations, calibrated to account for buckling interactions (Georgieva et al. 2012). Similar testing of varying cross-sections and DSM calibration was completed at the University of Hong Kong and attempts to efficiently model fasteners were studied and validated (Zhang 2014). Young and Chen (2008) conducted experiments on built-up CFS sections with intermediate stiffeners and explained that using the Direct Strength Method (DSM) for calculating nominal local and distortional capacities for only the single studs in a built-up section was adequate for providing reliable estimates of strength, and composite action was not thought to provide any strength increase, as seen in results of 3 ft (0.91 m) column tests completed by Fratamico et al. (2016). Craveiro et al. (2016) also reported on experimental work on back-to-back and closed section built-up CFS column capacities at lower and upper bounds using pin and fixed ends, respectively. AISI and Eurocode predictions of strength are shown to be conservative for fixed-ended columns, which is also seen in 6 ft (1.83 m) column tests reported in Fratamico et al. (2016). Buckling interactions are important in built-up CFS columns within and between individual studs per section. Li et al. (2014) completed experimental and numerical analyses of 2 types of screw-connected, built-up CFS sections made with both lipped and web-stiffened channel sections; additions to the AISI S100 (2012) design provisions for flexural and distortional buckling were recommended, and offered suggestions for optimal built-up member fastener spacing.

Built-up chord studs are important components of CFS structures, as indicated in experimental and numerical findings from the CFS-NEES effort by Schafer et al. (2016) and by work on the design of a CFS archetype structure by Torabian et al. (2016). In the latter work, the authors note that built-up chord studs should be designed for axial load and bending moments. Their flexural, torsional, and shear rigidities should be understood so that subsystems, such as shear walls, can be more properly modeled and designed. Also, larger stud packs are deemed undesirable, but common in design for multi-story CFS construction. The work presented herein is part of an ongoing experimental and numerical effort undertaken by the first author to understand and quantify the monotonic response of concentrically-loaded back-to-back built-up CFS columns that are bound by appropriately-sized tracks at their top and bottom ends to ensure true, semi-rigid end conditions as in practice. The tests presented in this paper were completed to understand the effects of end condition, web fastener layout, cross-section size, and steel plate thickness on the achievable composite action, prevailing buckling modes, and ultimate strength which can then be compared with estimates from existing design specifications.

2. Experimental Investigation

The tests reported here are part of a series of 3 phases of built-up CFS column tests at Johns Hopkins University. In this work, the effect of fastener layouts on the development of composite action in columns undergoing flexural buckling is studied. A total of 16 different cross-sections using a back-to-back shape (shown in Figure 1) are studied at a length of 6 ft (1.83 m). Monotonic, concentric compression loading was sought using a 100 kip (445 kN) MTS universal testing rig. The tests were displacement-controlled with a load rate not exceeding 0.015 in/min (0.38 mm/min). The column specimens are installed within tracks, which rest on fixed platen supports, as is shown in the following drawings. A total of 32 tests are performed, using two fastener layouts as discussed also in the next section.

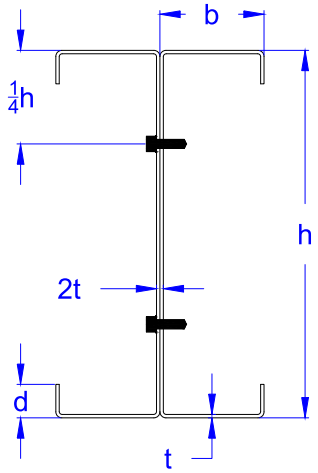

Figure 1. The back-to-back section studied, showing the location of the screw connections at the webs

2.1 Test Matrix

The primary motivation is to understand the effect of changing cross-sectional shape, plate thicknesses, and web fastener layout on composite action, observed buckling modes, and strength-to-squash load ratio. As mentioned earlier, two fastener layouts are used; the first case is a full, AISI-based layout with prescriptive end fastener groups (EFG) superimposed on an even spacing of L/4 as calculated using AISI S100 (2016), and the second case is with even fastener spacing but no EFG. Even fastener spacings are determined per AISI S100 (2016) sections I1.2 and J4.2 to be L/4, or 18 in. (457 mm) for all specimens. The length of the EFG from each end of the members were calculated as: 4.13 in. (105 mm), 5.44 in. (138 mm), and 9.00 in. (229 mm) for the specimens with 2.5 in. (63.5 mm), 3.625 in. (92.1 mm), and 6 in. (152 mm) web depths, respectively. EFG lengths are calculated as the maximum width of the column multiplied by 1.5. The 16 section types were selected based on the capacity of the MTS testing rig and with the intent of including a wide range of cross-section shapes commonly used for columns in CFS structures. Table 1 shows the test matrix and cross-sections selected.

Table 1. Test matrix

Trial ID	Section Designation[1]	Design Thickness mils (mm)				EFG[2] Installation	
		33 (0.88)	43 (1.15)	54 (1.44)	68 (1.81)	Yes	No
A1-33	250S137	X				X	
A1-43	250S137		X			X	
A1-54	250S137			X		X	
A1-68	250S137				X	X	
A2-33	250S137	X					X
A2-43	250S137		X				X
A2-54	250S137			X			X
A2-68	250S137				X		X
B1-33	362S137	X				X	
B1-43	362S137		X			X	
B1-54	362S137			X		X	
B1-68	362S137				X	X	
B2-33	362S137	X					X
B2-43	362S137		X				X
B2-54	362S137			X			X
B2-68	362S137				X		X
C1-33	600S137	X				X	
C1-43	600S137		X			X	
C1-54	600S137			X		X	
C1-68	600S137				X	X	
C2-33	600S137	X					X
C2-43	600S137		X				X
C2-54	600S137			X			X
C2-68	600S137				X		X
D1-33	600S162	X				X	
D1-43	600S162		X			X	
D1-54	600S162			X		X	
D1-68	600S162				X	X	
D2-33	600S162	X					X
D2-43	600S162		X				X
D2-54	600S162			X			X
D2-68	600S162				X		X

[1]Using AISI S200 nomenclature
[2]EFG refers to end fastener groups at the ends of columns

The lipped channel sections are connected together and to the corresponding track sections with steel-to-steel hex washer head screws (self-drilling size #10) for 54 mil (1.44 mm) and 68 mil (1.81 mm) specimens. For 33 mil (0.88 mm) and 43 mil (1.15 mm) specimens, the smaller sized #8 self-drilling screws are used instead.

2.2 Apparatus Setup and Instrumentation

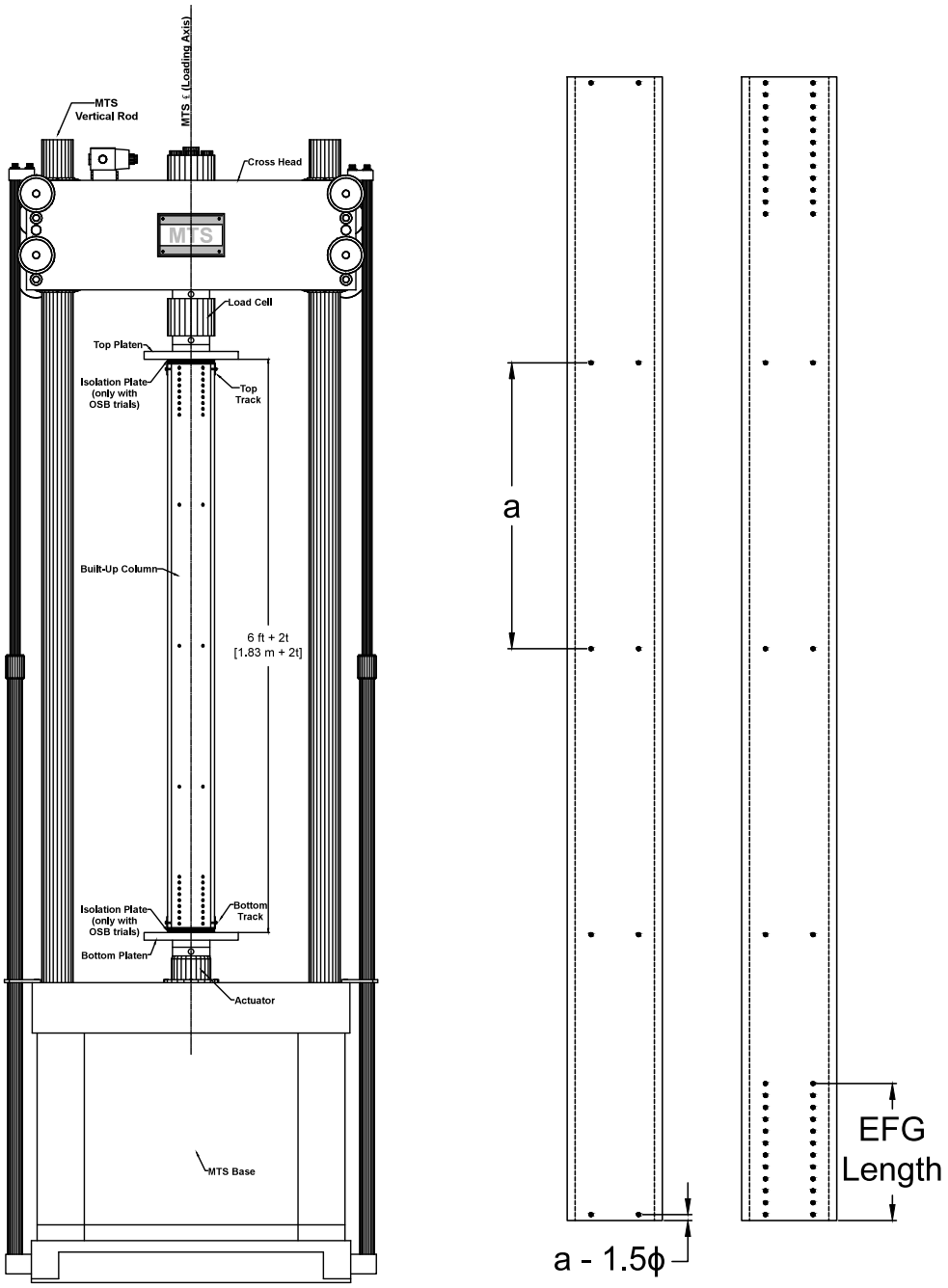

Figure 2. Elevation of test rig setup (left) and the two parametric fastener layouts used (right)

Figure 2 shows the MTS rig setup. Load is measured via a load cell installed at the top crosshead, and a built-in LVDT measures the applied displacements. LabVIEW software and National Instruments hardware are used to coordinate all data acquisition. Figure 2 also shows the parametric fastener layouts used for each section in the test series. Each section type is tested in two trials, as mentioned earlier: even fastener spacings and full AISI-based fastener layout with EFGs.

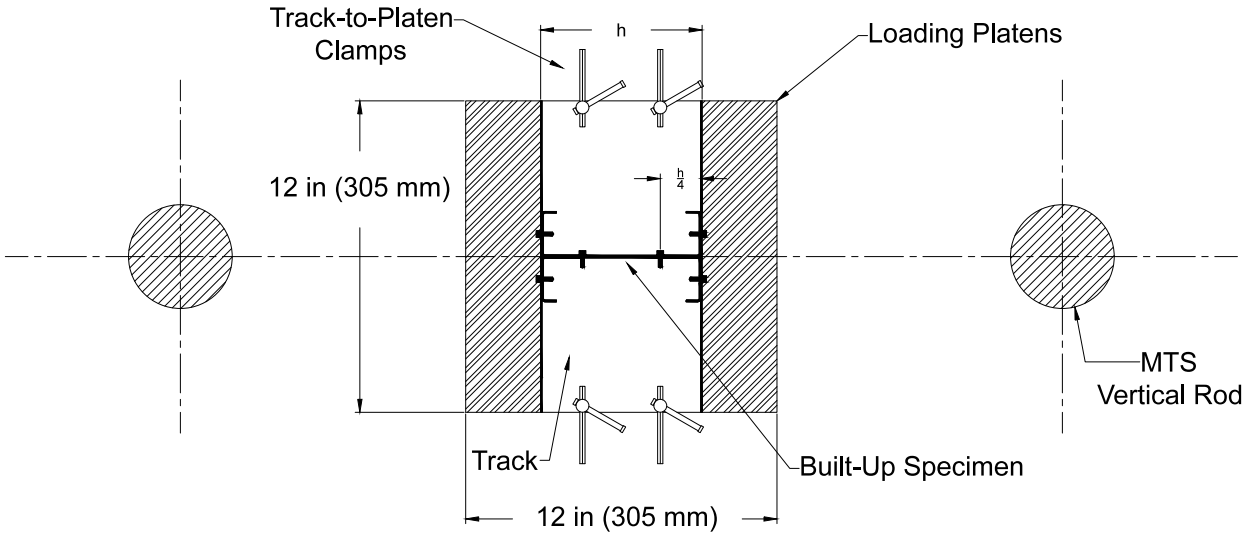

Figure 3. Placement of stud and track assembly on the loading platens (top-down view)

Loading platens are made of 0.5 in. (12.7 mm) thick low carbon steel and are installed parallel to each other with a maximum error of 0.05° from the horizontal plane. The positioning of the column in the rig is important, as concentric loads were sought in the tests. Figure 3 shows the placement of the specimens in the rig. Any errors of eccentricity and out-of-plumbness are recorded for each specimen as they are loaded into the rig, but were consistently less than 0.025 in. (0.64 mm). Measurements were taken in two planar directions at the top and bottom of the specimens to ensure that the centroids coincided with the line of action of the applied load in the rig.

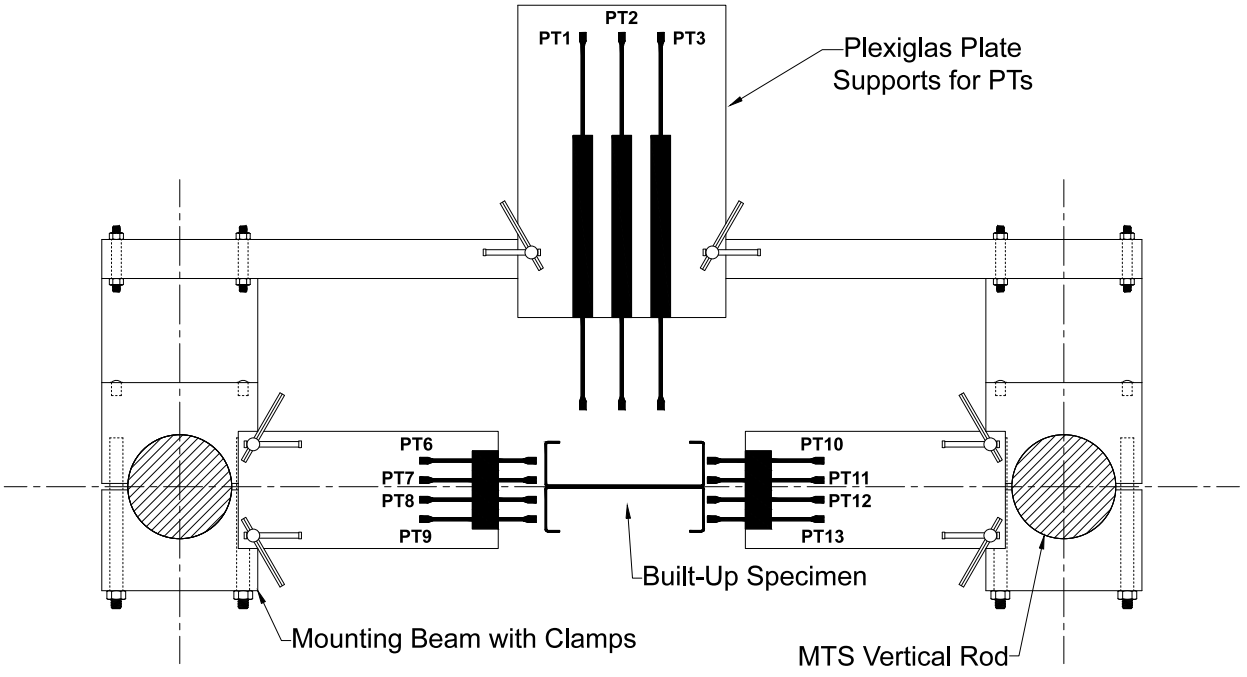

Figure 4. Placement of position transducers at mid-height (top-down view)

To track specimen deformations, 16 position transducers (PTs) are used. At mid-height, 11 PTs are used to measure lateral, bi-planar displacements and rotation of the specimen during the loading phase, as shown in Figure 4. The 12th and 13th PTs are installed on the web of the top and bottom tracks and orthogonal to the web of the column to measure out-of-plane deformation of the webs due to localized failures at either end of the column. To monitor stud engagement to the track during testing, the 14th and 15th PTs are installed: one at the top facing the top track web and one similarly at the bottom. Lastly, the 16th PT installed near the bottom (as shown in Figure 5) to monitor any relative slip between the two studs within the built-up section; the data is used as a direct measure of composite action. These PTs are only used in D-series tests, as those larger specimens allow for installation of this setup.

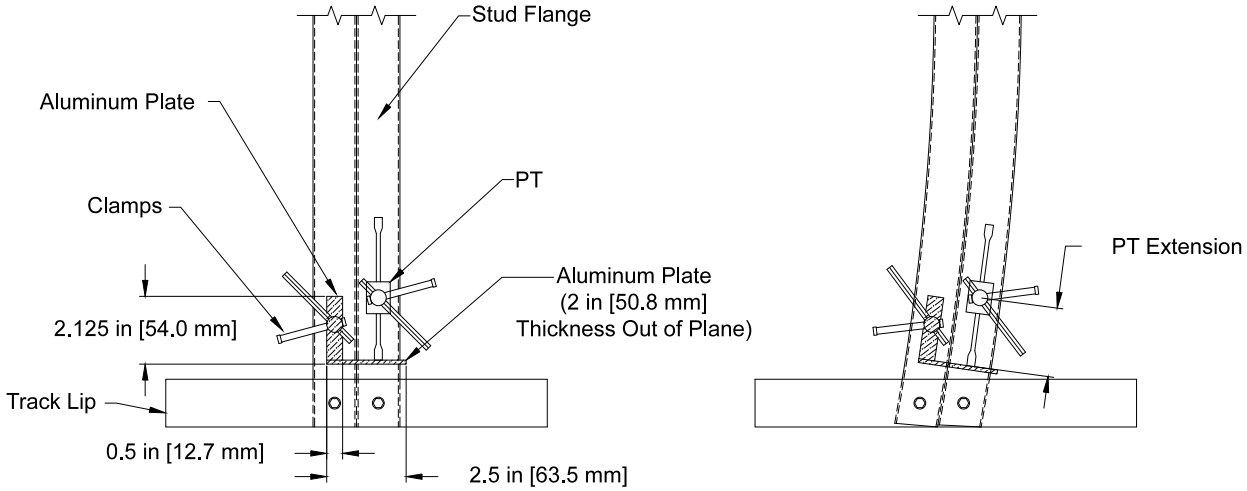

Figure 5. Setup for the "shear slip" position transducers in an undeformed state (left) and a deformed state (right)

2.3 Coupon Testing for Material Characterization

A series of 44 coupon tests were completed to quantify material properties of each section type used. Testing coupons were longitudinally cut from the webs and flanges (denoted as –W and –F, respectively, in the specimen names in Table 2) of each lipped channel type using a water jet cutter, and then milled with a CNC machine to correct ASTM A370-12a (2012) dimensions. Testing was completed in accordance with ASTM A370-12a (2012), and results are shown in Tables 2 and 3 for lipped channel and track sections, respectively. Measurements of coated and uncoated thickness were done, but specimens were first prepared; to remove the zinc coating at either end, both ends of all coupons were immersed in a 1M HCl solution until the coating was removed. Resulting yield stresses for the 33 mil (0.88 mm) and 43 mil (1.15 mm) thick sections manufactured with a specified yield stress of 33 ksi (228 MPa) were determined to be 46.4 ksi (320 MPa) and 48.3 ksi (333 MPa), respectively. For the sections with thicknesses of 54 mil (1.44 mm) and 68 mil (1.81 mm), yield stresses were determined to be 57.3 ksi (395 MPa) and 51.1 ksi (353 MPa), respectively. Coupons from track webs were also tested, but results are not shown here since yield stresses per plate thickness are very similar to the corresponding results from tests using coupons taken from the channel sections. Young's modulus is assumed to be 29,500 ksi (203 GPa) as prescribed in AISI S100 (2016).

Table 2. Tensile coupon test results from lipped channel sections

Specimen	Base Metal Thickness t (in) [mm]	Yield Stress* $F_{y,0.2}$ (ksi) [MPa]	Upper Yield Stress $F_{y,upper}$ (ksi) [MPa]	Ultimate Strength F_u (ksi) [MPa]	Strain at Ultimate Strength ε_u (in/in)
250S137-33-W	0.0353 [0.90]	44.0 [303]	44.2 [305]	56.9 [392]	0.232
250S137-33-F	0.0346 [0.88]	46.0 [317]	46.4 [320]	58.2 [401]	0.232
362S137-33-W	0.0338 [0.86]	48.8 [336]	51.0 [351]	56.2 [388]	0.201
362S137-33-F	0.0339 [0.86]	48.6 [335]	51.2 [353]	56.2 [387]	0.208
600S137-33-W	0.0349 [0.89]	46.1 [318]	50.4 [347]	53.3 [367]	0.232
600S137-33-F	0.0353 [0.90]	47.1 [325]	49.0 [338]	53.0 [366]	0.232
600S162-33-W	0.0340 [0.86]	43.0 [297]	43.4 [299]	53.4 [368]	0.207
600S162-33-F	0.0341 [0.87]	47.7 [329]	47.9 [330]	57.4 [396]	0.180
Mean	0.0345 [0.88]	46.4 [320]	47.9 [330]	55.6 [383]	0.215
C.o.V	0.019	0.045	0.063	0.037	0.091
250S137-43-W	0.0440 [1.12]	47.0 [324]	47.1 [324]	54.8 [378]	0.232
250S137-43-F	0.0444 [1.13]	45.8 [316]	46.0 [318]	54.3 [375]	0.223
362S137-43-W	0.0439 [1.12]	47.8 [330]	48.3 [333]	55.5 [383]	0.220
362S137-43-F	0.0439 [1.11]	48.7 [336]	49.0 [338]	55.8 [384]	0.230
600S137-43-W	0.0435 [1.10]	49.3 [340]	52.0 [359]	58.6 [404]	0.173
600S137-43-F	0.0437 [1.11]	49.2 [339]	51.8 [357]	58.3 [402]	0.170
600S162-43-W	0.0446 [1.13]	49.5 [341]	49.6 [342]	65.4 [451]	0.206
600S162-43-F	0.0445 [1.13]	48.9 [337]	49.3 [340]	65.3 [450]	0.211
Mean	0.0441 [1.12]	48.3 [333]	49.1 [339]	58.5 [403]	0.208
C.o.V	0.009	0.027	0.042	0.077	0.117
250S137-54-W	0.0579 [1.47]	63.4 [437]	64.5 [445]	76.5 [528]	0.191
250S137-54-F	0.0566 [1.44]	53.2 [367]	55.1 [380]	63.9 [441]	0.166
362S137-54-W	0.0543 [1.38]	56.2 [388]	56.5 [390]	70.5 [486]	0.175
362S137-54-F	0.0544 [1.38]	55.9 [385]	56.1 [387]	69.7 [480]	0.157
600S137-54-W	0.0551 [1.40]	57.7 [398]	57.9 [399]	69.8 [481]	0.177
600S137-54-F	0.0546 [1.39]	56.5 [389]	56.8 [392]	69.9 [482]	0.180
600S162-54-W	0.0549 [1.39]	57.9 [399]	57.9 [399]	69.7 [481]	0.176
600S162-54-F	0.0542 [1.38]	57.2 [395]	57.7 [398]	69.5 [480]	0.164
Mean	0.0553 [1.40]	57.3 [395]	57.8 [399]	69.9 [482]	0.173
C.o.V	0.024	0.050	0.050	0.046	0.062
250S137-68-W	0.0726 [1.85]	57.0 [393]	57.2 [394]	74.9 [516]	0.139
250S137-68-F	0.0728 [1.85]	57.8 [398]	57.8 [399]	74.9 [517]	0.146
362S137-68-W	0.0706 [1.79]	44.8 [309]	44.9 [309]	61.8 [426]	0.156
362S137-68-F	0.0709 [1.80]	48.5 [334]	48.6 [335]	67.5 [465]	0.165
600S137-68-W	0.0722 [1.83]	47.7 [329]	48.1 [332]	65.5 [452]	0.158
600S137-68-F	0.0727 [1.85]	49.7 [343]	50.0 [345]	65.5 [452]	0.168
600S162-68-W	0.0716 [1.82]	52.2 [360]	52.3 [361]	70.0 [483]	0.172
600S162-68-F	0.0719 [1.83]	51.4 [354]	51.5 [355]	69.7 [481]	0.156
Mean	0.0719 [1.83]	51.1 [353]	51.3 [354]	68.7 [474]	0.157
C.o.V	0.012	0.088	0.086	0.067	0.070

*The 0.2% offset method is used

2.4 Laser Scanning for the Quantification of Geometric Imperfections

Geometric imperfections were quantified using an in-house laser scanning rig at Johns Hopkins University. Full-field 3D geometric information is obtained as a point cloud of stitched longitudinal scan readings from multiple scan angles using an algorithm prepared by Zhao et al. (2015). For efficiency in model reconstruction, average plate thickness for each specimen was measured by hand using a calibrated micrometer and incorporated into the 3D geometry. Figure 6 shows the attainable imperfect cross-sectional dimensions and an example of the full-field 3D

reconstructed geometry of each specimen in the test series (Zhao and Schafer 2016). The data is currently being post-processed yet some scanned cross-section imperfection results for specimens with 54 mil (1.44 mm) plate thickness are shown in Table 3. Shell element meshes based on "true geometry" are also being developed and implemented in nonlinear FEA modeling.

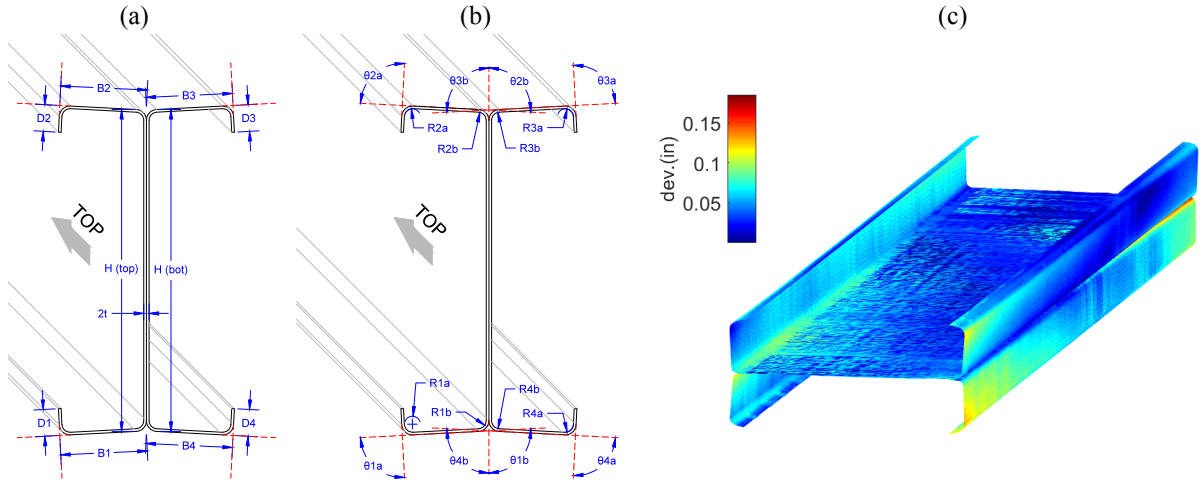

Figure 6. Results from laser scans: (a) imperfect cross-section linear dimensions averaged over full length, (b) averaged imperfect cross-section angles and radii, and (c) full-field 3D reconstruction of true geometry for FEA

Table 3. Mean cross-section dimensions* for select specimens using data from 561 cross-section readings per scan

Specimen	H_{top}	H_{bot}	B_1	B_2	B_3	B_4	D_1	D_2	D_3	D_4	R_{1a}	R_{1b}	R_{2a}
A1-54	2.52	2.51	1.31	1.34	1.31	1.34	0.38	0.39	0.37	0.37	0.18	0.18	0.18
B1-54	3.64	3.64	1.34	1.30	1.33	1.29	0.38	0.36	0.33	0.35	0.17	0.16	0.17
C1-54	6.00	6.00	1.34	1.28	1.28	1.32	0.41	0.41	0.39	0.40	0.17	0.13	0.18
D1-54	6.02	6.02	1.63	1.63	1.63	1.63	0.47	0.46	0.43	0.45	0.14	0.18	0.17
	R_{2b}	R_{3a}	R_{3b}	R_{4a}	R_{4b}	θ_{1a}	θ_{1b}	θ_{2a}	θ_{2b}	θ_{3a}	θ_{3b}	θ_{4a}	θ_{4b}
A1-54	0.18	0.19	0.15	0.23	0.18	100	89.9	97.0	90.8	102	89.0	97.0	91.1
B1-54	0.18	0.17	0.17	0.18	0.14	99.4	91.1	102	91.1	102	91.2	103	91.1
C1-54	0.19	0.18	0.14	0.21	0.16	98.2	92.3	102	91.8	103	91.7	96.6	92.0
D1-54	0.21	0.16	0.18	0.14	0.17	94.1	89.8	93.9	90.4	95.4	90.0	93.6	90.3

*Reported units: length in inches, angle in degrees

3. Experimental Results

3.1 Buckling Modes and Strength

At a height of 6 ft (1.83 m), all columns were expected to buckle in minor-axis flexural buckling. From general test observations, this hypothesis holds. However, local-global interaction was prevalent and in some cases, local-distortional-global interaction was observed. For some specimens with thinner steel plies, namely 33 mil (0.88 mm), localized failures near the flanges and lips caused premature collapse and governed post-peak deformations (and to view the test video for each trial, please visit *http://tinyurl.com/hhg3fn2*).

For specimens with smaller web depths of 2.5 in. (63.5 mm) and 3.625 in. (92.1 mm), a modest increase in capacity is observed when EFGs are added to the columns which buckle in a global mode with little local buckling interaction. For example, a 20% capacity boost is observed when comparing strengths of specimens A1-54 and A2-54. Also notable is the increase in interaction of local with minor-axis flexural buckling in trials with thinner steel plies, as shown in Figure 7.

These sections with thinner plies were also observed to have a capacity and deformation mode which was sensitive to geometric imperfections; examples of this are shown in Figures 7 & 9. In some cases, such as trials B1-33 (with EFG) and B2-33, no increase in strength was noted with the addition of the EFGs (depicted in Figure 8b), and a stronger presence of localized failure in lips and flanges (usually prior to flexural buckling) was instead noted during the tests.

Table 4. Test results for sections with web depths of 2.5 in. (63.5 mm)

Trial ID	SFIA Section Type	EFG Installed	Stiffness, k [kip/in] (kN/mm)[1]	Elastic Buckling Mode[2]	Tested Strength, P_u [kips] (kN)	P_u/P_y	$P_{u,EFG}/P_{u,noEFG}$
A1-33	250S137-33	Yes	116.7 (20.44)	L-G	10.38 (71.56)	0.57	1.11
A2-33	250S137-33	-	125.3 (21.94)	L-G	9.378 (64.66)	0.51	
A1-43	250S137-43	Yes	149.9 (26.24)	G	15.01 (103.5)	0.61	1.06
A2-43	250S137-43	-	143.4 (25.11)	G	14.16 (97.61)	0.57	
A1-54	250S137-54	Yes	196.5 (34.42)	G	25.51 (175.9)	0.71	1.20
A2-54	250S137-54	-	166.9 (29.23)	G	21.20 (146.2)	0.59	
A1-68	250S137-68	Yes	242.3 (42.44)	G	26.77 (184.6)	0.67	1.14
A2-68	250S137-68	-	221.2 (38.74)	G	23.54 (162.3)	0.59	

[1] The initial elastic stiffness, interpolated from raw data at the point after the studs engage with the tracks
[2] L = web local buckling and G = minor-axis flexural buckling

Table 5. Test results for sections with web depths of 3.625 in. (92.1 mm)

Trial ID	SFIA Section Type	EFG Installed	Stiffness, k [kip/in] (kN/mm)	Elastic Buckling Mode	Tested Strength, P_u [kips] (kN)	P_u/P_y	$P_{u,EFG}/P_{u,noEFG}$
B1-33	362S137-33	Yes	119.4 (20.90)	L-G	9.964 (68.70)	0.45	0.99
B2-33	362S137-33	-	88.01 (15.41)	L-G	10.03 (69.12)	0.46	
B1-43	362S137-43	Yes	173.0 (30.30)	L-G	15.89 (109.6)	0.54	1.16
B2-43	362S137-43	-	123.8 (21.68)	L-G	13.71 (94.56)	0.46	
B1-54	362S137-54	Yes	214.4 (37.55)	L-G	23.15 (159.6)	0.53	1.15
B2-54	362S137-54	-	165.4 (28.96)	L-G	20.17 (139.1)	0.46	
B1-68	362S137-68	Yes	237.9 (41.66)	G	26.06 (179.7)	0.54	1.42
B2-68	362S137-68	-	128.6 (22.51)	G	18.37 (126.6)	0.38	

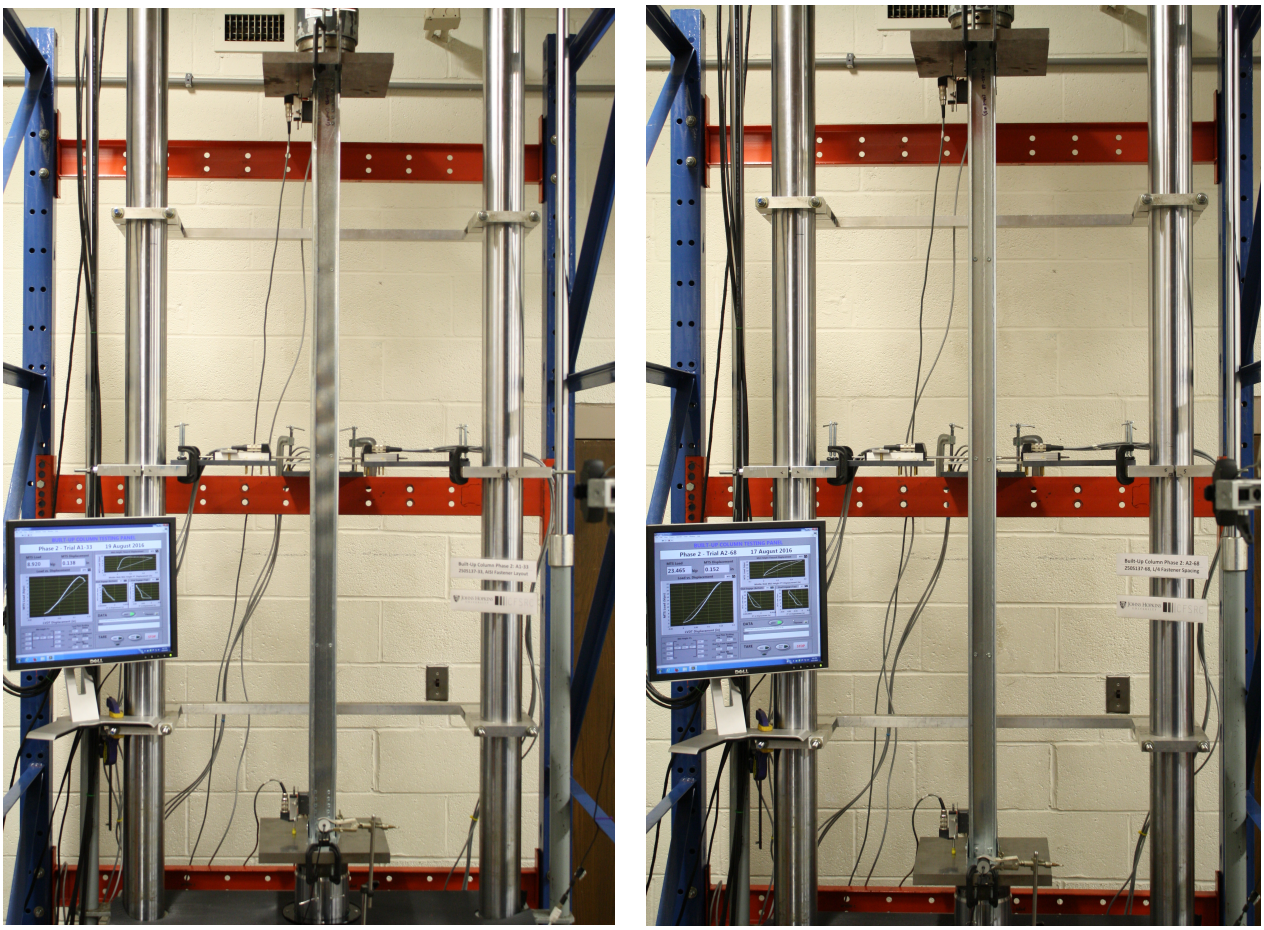

Figure 7. Local-flexural interaction in trial A1-33 (left) and minor-axis flexural deformation in trial A2-68 (right)

As plate thickness increased, less interaction of local buckling with flexural buckling was observed, and the effect of EFG on increasing both capacity (in fact, up to 42% increase for B1-68 and B2-68) and stiffness was also greater. This is shown in Table 5 and both plots in Figure 8 for specimens with 68 mil (1.81 mm) thick plies.

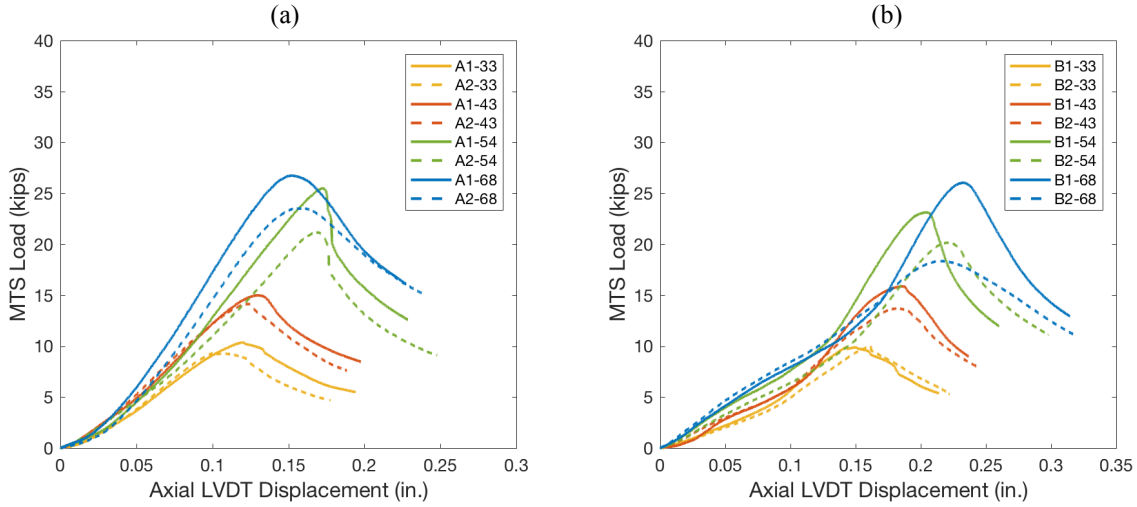

Figure 8. Load vs. axial displacement curves for (a) A and (b) B series specimens, with solid and dashed lines representing specimens with and without EFG, respectively

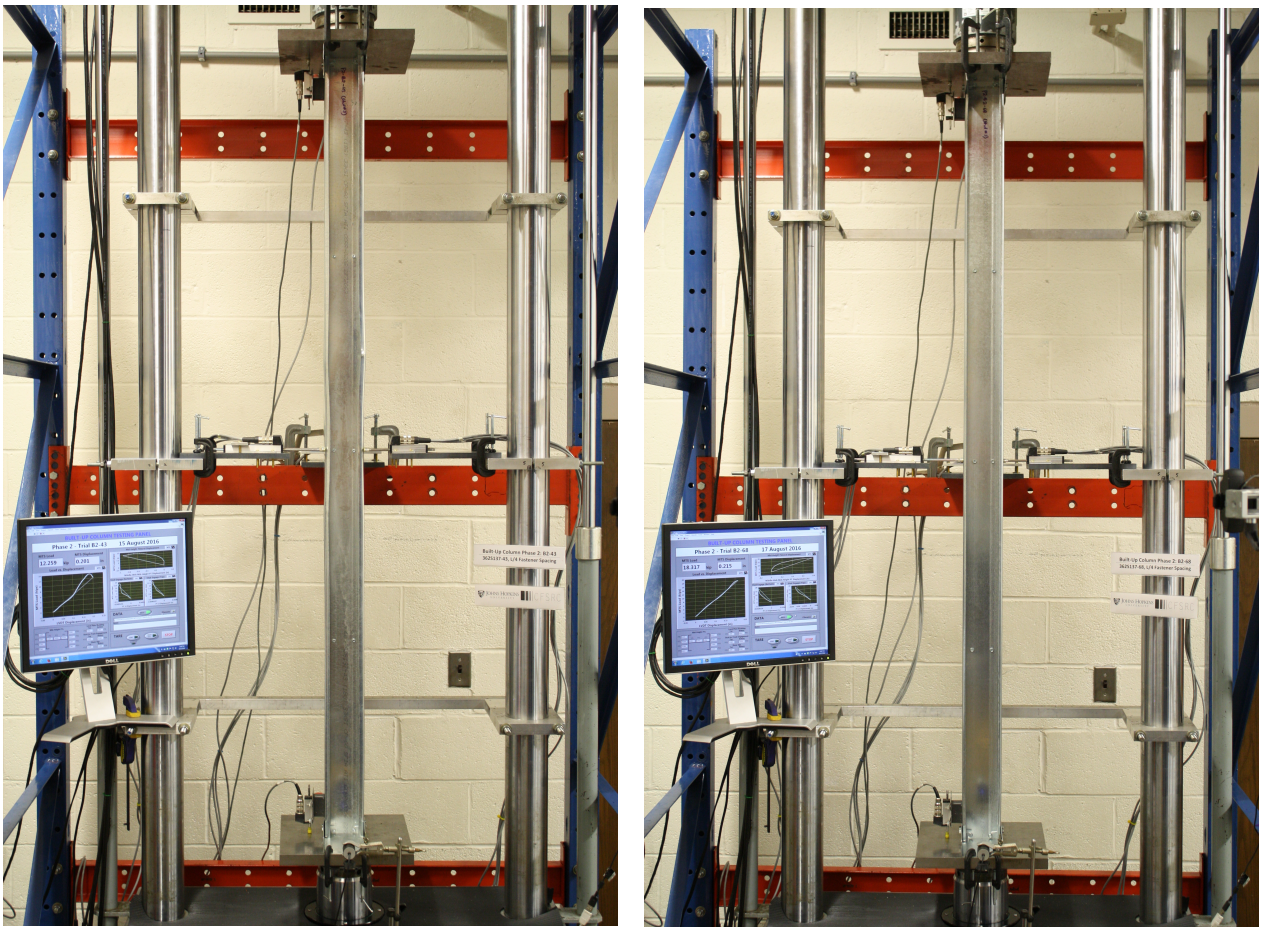

Figure 9. Localized failures in trial B2-43 (left) and minor-axis flexural deformation in trial B2-68 (right)

Figures 8 and 11 show an approximately bi-linear stiffness before peak. This is attributed to the early stages of loading in which the column end conditions change as the ends of the studs bear down onto the webs of the track. This type of end condition nonlinearity was most prevalent in the B, C, and D series trials with cross-sections with web depths of 3.625 in. (92.1 mm) and 6 in. (152 mm). The effect is intentional in all specimens to ensure a more realistic column loading condition. Position transducers were placed at the top and bottom tracks to monitor this stud seating in the track (zero PT displacement), as shown in the example raw data in Figure 10.

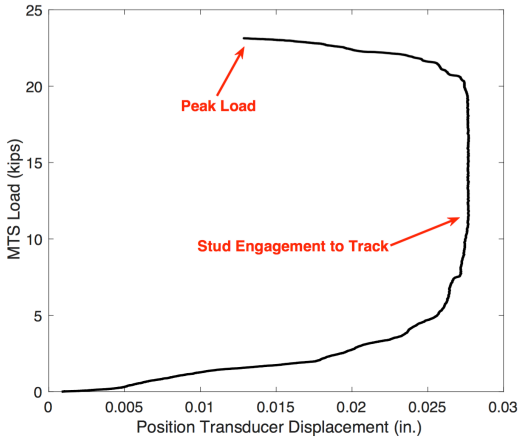

Figure 10. Example of the engagement of column C1-54 with bottom track using PT #14 data

Tables 6 and 7 provide results for all sections with web depths of 6 in. (152 mm). Stiffness increases with the addition of EFGs, and capacity also increases with the EFGs in the sections with thicker plies. For example, a 33.3% increase in capacity is observed in trial C1-68 when compared with C2-68 which did not have EFG installed. This boost in capacity, as reported earlier for sections with shorter web depths, is not as prevalent in sections with thinner plies.

Table 6. Test results for sections with web depths of 6 in. (152 mm) and flange widths of 1.375 in. (34.9 mm)

Trial ID	SFIA Section Type	EFG Installed	Stiffness, k [kip/in] (kN/mm)[1]	Elastic Buckling Mode[2]	Tested Strength, P_u [kips] (kN)	P_u/P_y	$P_{u,EFG}/P_{u,noEFG}$
C1-33	600S137-33	Yes	130.7 (22.88)	L-G	11.29 (77.87)	0.38	0.96
C2-33	600S137-33	-	99.46 (17.42)	L-G	11.72 (80.82)	0.40	
C1-43	600S137-43	Yes	182.0 (31.87)	L-G	17.69 (122.0)	0.44	1.11
C2-43	600S137-43	-	200.3 (35.07)	L-G	15.92 (109.8)	0.40	
C1-54	600S137-54	Yes	277.0 (48.52)	L-G	23.18 (159.8)	0.39	1.14
C2-54	600S137-54	-	259.0 (45.36)	L-G	20.39 (140.6)	0.35	
C1-68	600S137-68	Yes	335.1 (58.69)	L-G	33.97 (234.2)	0.52	1.33
C2-68	600S137-68	-	323.1 (56.59)	L-G	25.49 (175.7)	0.39	

[1] The initial elastic stiffness, interpolated from raw data at the point after the studs engage with the tracks
[2] L = web local buckling and G = minor-axis flexural buckling

Table 7. Test results for sections with web depths of 6 in. (152 mm) and flange widths of 1.625 in. (41.3 mm)

Trial ID	SFIA Section Type	EFG Installed	Stiffness, k [kip/in] (kN/mm)	Elastic Buckling Mode	Tested Strength, P_u [kips] (kN)	P_u/P_y	$P_{u,EFG}/P_{u,noEFG}$
D1-33	600S162-33	Yes	122.8 (21.50)	L-G	11.06 (76.25)	0.35	1.01
D2-33	600S162-33	-	118.2 (20.69)	L-G	10.91 (75.20)	0.34	
D1-43	600S162-43	Yes	175.7 (30.77)	L-G	16.17 (111.5)	0.37	0.95
D2-43	600S162-43	-	186.2 (32.61)	L-G	17.00 (117.2)	0.39	
D1-54	600S162-54	Yes	275.6 (48.26)	L-G	30.97 (213.5)	0.49	1.22
D2-54	600S162-54	-	217.3 (38.06)	L-G	25.34 (174.7)	0.40	
D1-68	600S162-68	Yes	373.6 (65.43)	L-G	39.24 (270.5)	0.55	1.06
D2-68	600S162-68	-	301.7 (52.83)	L-G	36.97 (254.9)	0.52	

When comparing capacity for the C and D series trials (differing flange widths), the ratios of capacity normalized to squash loads remain around 0.4, and generally less than 0.55 for stockier sections. For these 16 trials, local-global interaction was observed, and in some cases, a local-distortional-global interaction occurred and was noticeable at peak load, as shown in Figure 12.

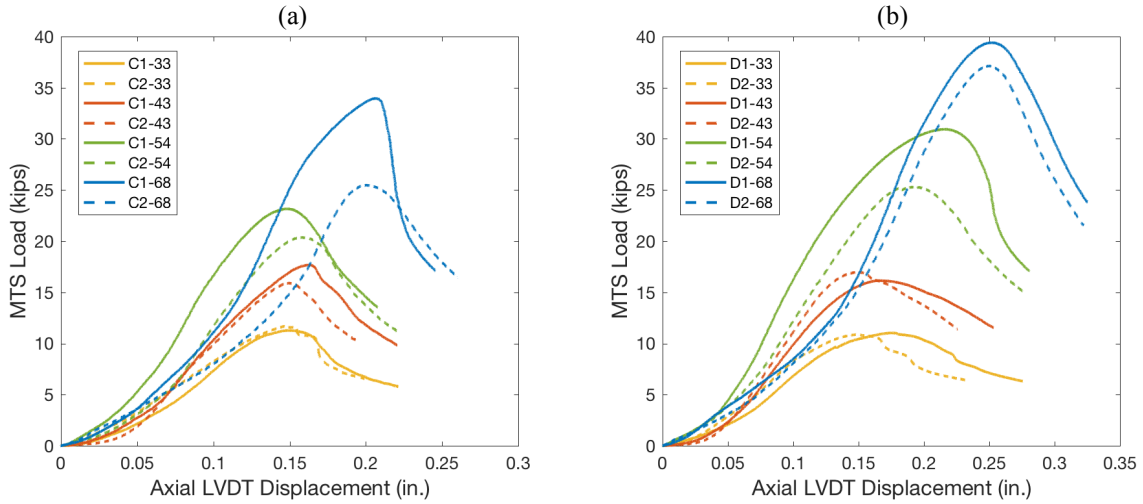

Figure 11. Load vs. axial displacement curves for (a) C and D series specimens, with solid and dashed lines representing specimens with and without EFG, respectively

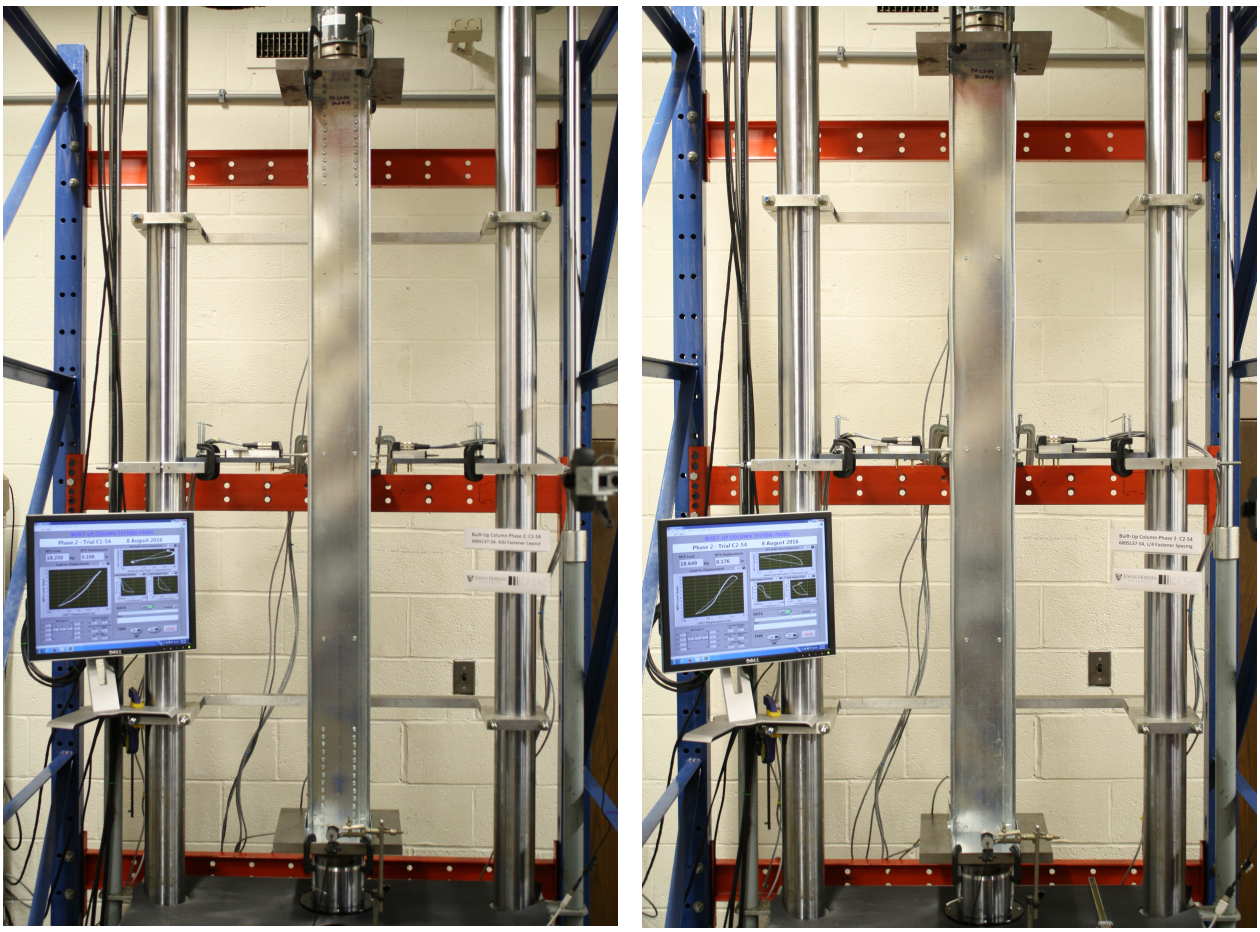

Figure 12. Local-flexural buckling in trial C1-54 (left), local-distortional-flexural interaction in trial C2-54 (right)

Figure 13. Side view of (a) a semi-rigid condition at peak load and (b) corresponding lip/flange lift-off for C2-54

End conditions were closely monitored with cameras and position transducers throughout the entire loading phase. After stud engagement to track, an additional source of end condition nonlinearity was observed in most trials. Occurring just after peak when flexural deformations are amplified, lips and a portion of flanges on the concave side of the column lift off from the tracks, changing not only the stress distribution on the cross section, but also reducing the rigidity of the end condition. Figure 13 shows an example of the semi-rigid end condition and the change in cross section bearing on the track web, which is not present in most other built-up CFS column tests in the literature as they employ fixed ends. In successive work, quantification of end rigidity of all the columns tested will be completed using the Southwell (1932) or similar method.

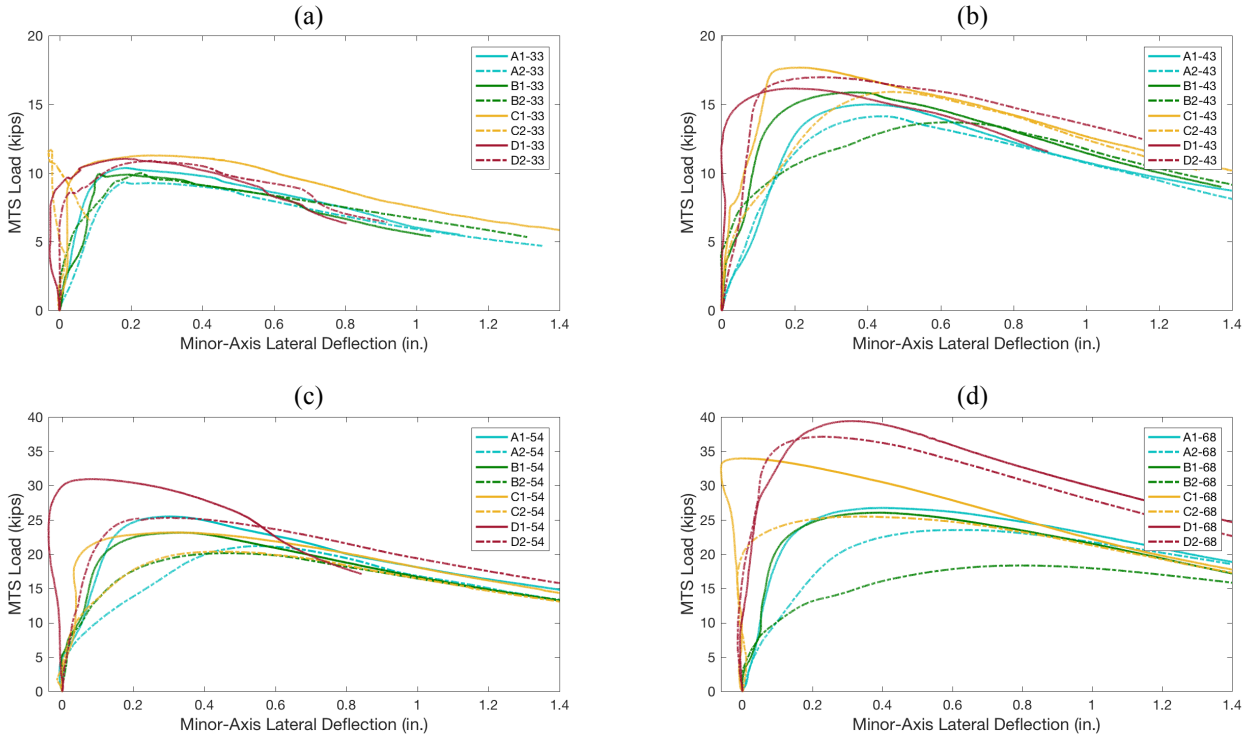

Figure 14. Load vs. mid-height lateral deflection curves for all specimens (one plate thickness is represented per plot), with solid and dashed lines representing specimens with and without EFG, respectively

In Figure 14, plots of load vs. the lateral deflection at mid-height are shown, and results across section type can be made for each plate thickness. In many trials, the lateral deflection changed sign through the initial loading phase due to the interaction of local and global buckling waves at the location of the PT, before measuring the progression of the flexural buckling deflection. As expected, with local-global buckling interaction prevailing in the whole test series, the largest section (the D series specimens), which had the largest minor-axis moment of, reached the highest capacity. However, the presence of the EFG did not boost the capacity in these sections. Figure 14 also indicates that a wide range of column stiffness and initial flexural imperfections, coupled with the nonlinear end conditions, deserves further study.

Although load-axial displacement data shows the effect of composite action on stiffness and strength, direct measurements of shear slip between the screw-connected webs were made using a special position transducer setup on all D series specimens (PT #16 mentioned previously). As an example, only 43 mil and 54 mil (1.15 mm and 1.44 mm, respectively) specimens are shown in Figure 15. When fastener groups are installed at the points of maximum shear slip in members in flexure, the slip between the webs is greatly reduced, as shown by the reduced travel in the blue curves in Figure 15.

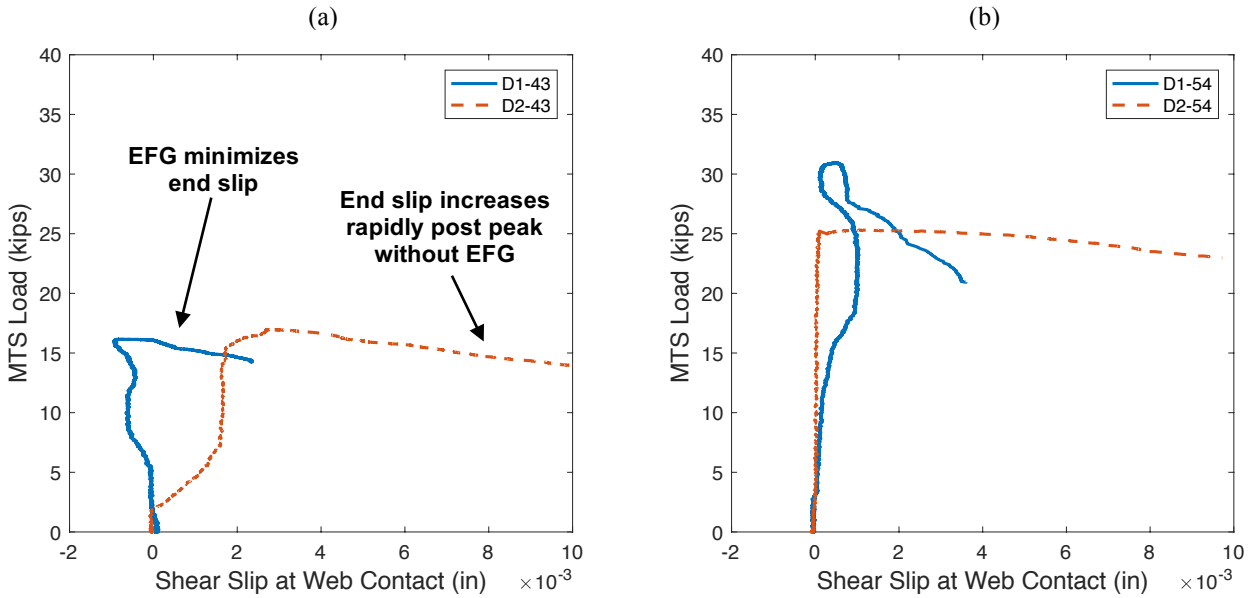

Figure 15. Load vs. shear slip curves showing the amount of slippage between webs from initial loading to collapse), with solid and dashed lines representing specimens with and without EFG, respectively

3.2 Comparison with DSM Predictions

As a means of initial comparison with experimental results, models of each section type were created and analyzed using elastic buckling, finite strip-based software CUFSM (Schafer and Ádány 2006). Each section was made using the actual plate thickness measured in tensile testing coupons and recorded in Table 2. Four strips were used in the lips, flanges, and corners, and eight strips were used for the webs. To model the web fasteners, a simple 4 DOF fixed constraint between web nodes were used; the placement of these master-slave type constraints correspond to the locations in which screws were installed in the tested specimens. Two end conditions were used in the models: a pinned condition using a signature curve analysis and a clamped condition using a generalized boundary condition method (in which significant modal interaction may exist

when searching for local, distortional, and global buckling modes). A total of 16 analyses were completed, and the Direct Strength Method (DSM) in AISI S100 (2016) was used to estimate strength for all columns. Tables 8 and 9 show the comparison of DSM results (using both pinned and clamped end buckling analysis results) and test data.

Table 8. Comparison of test results with DSM strength predictions, for tested specimens with EFG

Trial	SFIA Section	Test Results		DSM with Pinned Ends			DSM with Clamped Ends		
		P_u/P_y	Mode	P_n/P_y	Mode	$\mathbf{P_{u,test}/P_n}$	P_n/P_y	Mode	$\mathbf{P_{u,test}/P_n}$
A1-33	250S137-33	0.57	L-G	0.48	G	**1.18**	0.65	L-G	**0.87**
A1-43	250S137-43	0.61	G	0.44	G	**1.37**	0.71	L-G	**0.86**
A1-54	250S137-54	0.71	G	0.32	G	**2.23**	0.63	G	**1.11**
A1-68	250S137-68	0.67	G	0.38	G	**1.77**	0.72	G	**0.93**
B1-33	362S137-33	0.45	L-G	0.33	L-G	**1.38**	0.51	L-G	**0.89**
B1-43	362S137-43	0.54	L-G	0.36	L-G	**1.51**	0.58	L-G	**0.92**
B1-54	362S137-54	0.53	L-G	0.27	G	**1.96**	0.50	L-G	**1.07**
B1-68	362S137-68	0.54	G	0.33	G	**1.65**	0.70	L-G	**0.77**
C1-33	600S137-33	0.38	L-G	0.22	L-G	**1.75**	0.36	L-G	**1.06**
C1-43	600S137-43	0.44	L-G	0.24	L-G	**1.84**	0.44	L-G	**1.00**
C1-54	600S137-54	0.39	L-G	0.20	L-G	**2.00**	0.41	L-G	**0.97**
C1-68	600S137-68	0.52	L-G	0.28	G	**1.84**	0.51	L-G	**1.02**
D1-33	600S162-33	0.35	L-G	0.25	L-G	**1.36**	0.33	L-G	**1.04**
D1-43	600S162-43	0.37	L-G	0.29	L-G	**1.30**	0.41	L-G	**0.91**
D1-54	600S162-54	0.49	L-G	0.24	L-G	**1.99**	0.39	L-G	**1.26**
D1-68	600S162-68	0.55	L-G	0.36	L-G	**1.53**	0.56	L-G	**0.98**
	Mean					**1.67**			**0.98**
	C.o.V.					**0.181**			**0.119**

Table 9. Comparison of test results with DSM strength predictions, for test specimens without EFG

Trial	SFIA Section	Test Results		DSM with Pinned Ends			DSM with Clamped Ends		
		P_u/P_y	Mode	P_n/P_y	Mode	$\mathbf{P_{u,test}/P_n}$	P_n/P_y	Mode	$\mathbf{P_{u,test}/P_n}$
A2-33	250S137-33	0.51	L-G	0.48	G	**1.06**	0.65	L-G	**0.79**
A2-43	250S137-43	0.57	G	0.44	G	**1.30**	0.71	L-G	**0.82**
A2-54	250S137-54	0.59	G	0.32	G	**1.85**	0.63	G	**0.93**
A2-68	250S137-68	0.59	G	0.38	G	**1.56**	0.72	G	**0.82**
B2-33	362S137-33	0.46	L-G	0.33	L-G	**1.39**	0.51	L-G	**0.90**
B2-43	362S137-43	0.46	L-G	0.36	L-G	**1.31**	0.58	L-G	**0.80**
B2-54	362S137-54	0.46	L-G	0.27	G	**1.70**	0.50	L-G	**0.93**
B2-68	362S137-68	0.38	G	0.33	G	**1.16**	0.70	L-G	**0.54**
C2-33	600S137-33	0.40	L-G	0.22	L-G	**1.81**	0.36	L-G	**1.10**
C2-43	600S137-43	0.40	L-G	0.24	L-G	**1.65**	0.44	L-G	**0.90**
C2-54	600S137-54	0.35	L-G	0.20	L-G	**1.75**	0.41	L-G	**0.86**
C2-68	600S137-68	0.39	L-G	0.28	G	**1.38**	0.51	L-G	**0.76**
D2-33	600S162-33	0.34	L-G	0.25	L-G	**1.34**	0.33	L-G	**1.03**
D2-43	600S162-43	0.39	L-G	0.29	L-G	**1.37**	0.41	L-G	**0.96**
D2-54	600S162-54	0.40	L-G	0.24	L-G	**1.63**	0.39	L-G	**1.03**
D2-68	600S162-68	0.52	L-G	0.36	L-G	**1.44**	0.56	L-G	**0.93**
	Mean					**1.48**			**0.88**
	C.o.V.					**0.158**			**0.149**

Considering the constraints as an efficient fastener model, and pinned and clamped ends representing a lower and upper bound condition, respectively, the DSM buckling modes mostly matched those observed in the tests. Although a full quantification of the semi-rigid end condition for each specimen is not yet complete, a comparison of nominal capacities using DSM with tested

capacities reveals that a clamped condition most closely approximates the end condition of back-to-back CFS sections, with local-global interaction as the prevailing failure mode. There exist outliers, such as a $P_{u,test}/P_n$ of 0.54 for specimen B2-68 in Table 9 which could be attributed to improper stud-to-track seating and imperfections in that specimen. Modeling using pinned ends does consistently underestimate capacity, so a signature curve analysis is inadequate for design.

4. Discussion

Results from the tests show that with smaller plate thickness, global buckling occurs but localized failures due to small geometric imperfections accompanied the flexural deformation and reduced capacity. This effect was evident in the D series specimens with 1.625 in. (41.3 mm) wide flanges. Sections with thicker plies had a clearer flexural buckling behavior, but some local-global interaction was still observed (and estimated by CUFSM analyses and DSM). Thus, the effect of the EFG was greater since shear slip was reduced and composite action therefore increased. In previous work, the first author conducted CUFSM analyses considering various methods of fastening sections together in a finite strip modeling framework, and showed that, fastener layouts and level of composite action do not boost local and distortional buckling capacities (Fratamico and Schafer 2014). The authors reached a similar conclusion in 3 ft (0.91 m) built-up CFS columns tests (Fratamico et al. 2016). EFGs and other built-up stud fastener layouts appear to considerably boost only global buckling capacity.

DSM estimates of nominal capacity, which required elastic buckling results from fixed end models, generally compared favorably with tested capacities. The true end conditions are semi-rigid, but closest to a fixed condition; test observations confirm this. Therefore, a signature curve analysis in finite strip-based elastic buckling software may yield overly conservative estimates of buckling capacity, and consequently overly conservative strength values if unmodified. The tests also show a range of stud to track connection behavior, as well as reveal uncertainties in end conditions for cold-formed steel studs bearing on tracks. Also, stud lift-off from track during flexural buckling is potentially a problem, as a reduced load bearing area of the cross section can reduce the overall capacity of members.

Geometric imperfections are not considered in the treatment of test data, but laser scans of all tested sections were completed and are currently used in finite element analyses that consider geometric and material nonlinearity. The goal is to use true geometry and a material model based on coupon tests to create models with fidelity that validate well with test results; the motivation is to continue to analyze more complex built-up CFS section types, perform studies aimed at reducing the complexity of fastener layouts, and potentially study the behavior of perforated built-up sections in compression or bending.

5. Conclusions

Understanding the behavior and strength of screw-fastened built-up cold-formed steel (CFS) columns is important, as they are used with increasing frequency in CFS framing. The test series presented herein was developed to analyze a range of section types, fastened in a common back-to-back built-up section; fastener layouts were studied and cross-compared with section types and steel plate thicknesses. A costly end fastener grouping consisting of a large series of fasteners at the member ends is shown to boost the capacity of columns only when buckling in minor-axis flexure, but even then, only a limited boost. As most columns in CFS structures are sheathed and/or

braced, local and distortional buckling dominate the failure mode and column capacity, and therefore the EFGs are not important. Ongoing work aims to develop better design methods that incorporate more accurate estimations of column end conditions and explicit modeling of web fasteners. In doing so, the feasibility of partially-composite column curves can then be fully assessed.

Acknowledgements

Research for this paper was conducted with partial U.S. Government support under FA9550-11-C-0028 and awarded by the Department of Defense, Air Force Office of Scientific Research, National Defense Science and Engineering Graduate (NDSEG) Fellowship, 32 CFR 168a. The senior authors would also like to acknowledge support from the Australian Research Council for collaboration on this topic under Discovery Project DP140104464. Special thanks to Nick Logvinovsky for his assistance in lab apparatus repairs and upgrades. The first author is very grateful for his lab assistants Xiaomeng Li, Avi Gordon, and Matthew Brandes for their help in specimen preparation, laser scanning work, and coupon testing. Lastly, thanks to ClarkDietrich Building Systems and Simpson Strong-Tie for graciously providing all CFS sections and screw fasteners, respectively. Any opinions, findings, and conclusions or recommendations expressed in this material are those of the author(s) and do not necessarily reflect the views of the sponsors or other participants.

References

AISC 360 (2010). *Specification for Structural Steel Buildings*, American Institute of Steel Construction, Chicago, IL.

AISI S100. (2016). *North American Specification for the Design of Cold-Formed Steel Structural Members*, American Iron and Steel Institute, Washington, D.C.

American Society for Testing and Materials (ASTM), Standard Test Methods and Definitions for Mechanical Testing of Steel Products (ASTM370-12a), ASTM, West Conshohocken, PA, 2012.

Craveiro, H.D., Paulo, J., Rodrigues, C., and Laím, L. (2016). "Buckling resistance of axially loaded cold-formed steel columns." *Thin-Walled Structures*, 106, 358-375.

Fratamico, D.C. and Schafer, B.W. (2014). "Numerical Studies on the Composite Action and Buckling Behavior of Built-Up Cold-Formed Steel Columns." 22nd Int'l. Spec. Conf. on Cold-Formed Steel Structures, St. Louis, MO.

Fratamico, D.C., Torabian, S., Rasmussen, K.J.R., Schafer, B.W. (2016). "Experimental Investigation of the Effect of Screw Fastener Spacing on the Local and Distortional Buckling Behavior of Built-Up Cold-Formed Steel Columns." Proc. of the Wei-Wen Yu International Specialty Conference on Cold-Formed Steel Structures, Baltimore, MD.

Fratamico, D.C., Torabian, S., Rasmussen, K.J.R., Schafer, B.W. (2016). "Experimental Studies on the Composite Action in Wood-Sheathed and Screw-Fastened Built-Up Cold-Formed Steel Columns." Proc. of the Annual Stability Confrence, Structural Stability Research Council, Orlando, FL.

Georgieva, I., Schueremans, L., Pyl, L., Vandewalle, L. (2012). "Experimental investigation of built-up double-Z members in bending and compression." *Thin-Walled Structures*, 53, 48-57.

Georgieva, I., Schueremans, L., Vandewalle, L., Pyl, L. (2012). "Design of built-up cold-formed steel columns according to the direct strength method." *Procedia Engineering*, 40, 119-124.

LaBoube, R. (2016). "Cold-Formed Steel – Research to Practice." Proc. of the Annual Stability Confrence, Structural Stability Research Council, Orlando, FL.

Li, Yuanqi, Li, Yinglei, Wang, S., Shen, Z. (2014). "Ultimate load-carrying capacity of cold-formed thin-walled columns with built-up box and I section under axial compression." *Thin-Walled Structures*, 79, 202-217.

Li, Z. and Schafer, B.W. (2010a). "Buckling analysis of cold-formed steel members with general boundary conditions using CUFSM: conventional and constrained finite strip methods." Proc. of the 20th International Specialty Conference on Cold-Formed Steel Structures, St. Louis, MO.

Schafer, B.W. and Ádány, S. (2006). "Buckling analysis of cold-formed steel members using CUFSM: conventional and constrained finite strip methods." Proc. of the 18th International Specialty Conference on Cold-Formed Steel Structures, Orlando, FL.

Schafer, B.W., Ayhan, D., Leng, J., Liu, P., Padilla-Llano, D., Peterman, K.D., Stehman, M., Buonopane, S.G., Eatherton, M.m Madsen, R., Manley, B., Moen, C.D., Nakata, N., Rogers, C., and Yu, C. (2016). "Seismic Response and Engineering of Cold-formed Steel Framed Buildings." *Structures*, 8 (2), 197-212.

Southwell, R.V. (1932). "On the analysis of experimental observations in problems of elastic stability." *Proceedings of the Royal Society of London A: Mathematical, Physical and Engineering Sciences*. 135 (828), 601-616.

Stone, T.A. and LaBoube, R.A. (2005). "Behavior of cold-formed steel built-up I-sections." *Thin-Walled Structures*, 43(12), 1805-1817.

Torabian, S., Saneei Nia, Z., and Schafer, B.W. (2016). "An Archetype Mid-Rise Building for Novel Complete Cold-Formed Steel Buildings." Proc. of the Wei-Wen Yu International Specialty Conference on Cold-Formed Steel Structures, Baltimore, MD.

Torabian, S., Zheng, B., and Schafer, B.W. (2015). "Experimental response of cold-formed steel lipped channel beam-columns" Thin-Walled Structures, 89, 152-168.

Young, B. and Chen, J. (2008). "Design of Cold-Formed Steel Built-Up Closed Sections with Intermediate Stiffeners." *Journal of Structural Engineering*, 134, 727-737.

Zhang, J. *Cold-formed steel built-up compression members with longitudinal stiffeners*. Ph.D. Thesis, The University of Hong Kong; 2014.

Zhao, X. and Schafer, B.W. (2016). "Measured geometric imperfections for Cee, Zee, and Built-up cold-formed steel members." Proc. of the Wei-Wen Yu International Specialty Conference on Cold-Formed Steel Structures, Baltimore, MD.

Zhao, X., Tootkaboni, M., Schafer, B.W. (2015). "Development of a Laser-Based Geometric Imperfection Measurement Platform with Application to Cold-Formed Steel Construction." *Experimental Mechanics*, 55, 1779-1790.